ADVANCED COMPOSITE MATERIALS FOR SUPPRESSING FLOW-INDUCED VIBRATIONS IN DISTENSIBLE TUBES

Kizilova N.,[1] *Hamadiche M.*,[2] *Gad-el-Hak M.*[3]

[1]Kharkov National University, Ukraine
[2]Ecole Centrale de Lyon, France
[3]Virginia Commonwealth University, Richmond, USA

Examples of fluid flows in collapsible ducts and over compliant surfaces are abound in technological applications, e.g. fluid separation, drug purification, and polymer processing; in living organisms, e.g. flow in blood vessels, urine motion in urethra, air flow through nasal cavities, vocal cord, bronchi, and upper airways; and in machinery such as aircrafts, underwater vehicles, and turbine blades. Instability of the steady flow of a viscous incompressible liquid near a compliant wall may produce wall oscillations, flow and pressure limitation phenomena, noise generation, fatigue of the wall material, and even destruction of the device. Delaying the onset of the instability, laminar-to-turbulence transition, and stabilization of the unstable modes pose a challenging problem to both theoretical mechanics and mechanical engineering. Flow stability in isotropic compliant tubes has been studied in-depth in experiments and numerical computations using one-dimensional and two-dimensional mathematical models [1–5]. Passive control over the system stability and noise suppression in rigid ducts by flush-mounted panels has been proposed in [6]. More recently, [7,8] consider active control in blood vessels for short-time via contraction of smooth-muscle cells in vessel walls, variation of vessel lumen, and wall thickness and rigidity, and long-time via cell orientation, wall remodeling, and physiological mechanisms become more important [7,8].

Though many physical and physiological phenomena related to flow instabilities in collapsed and non-collapsed tubes are explained, the problem is still of great interest in relation to different technical and biomedical applications, especially from the standpoint of sound generation and flow control in biological organisms and technical devices [7–10].

Some important proposals for the tube wall structure and geometry needed for the flow stabilization and vibration quenching can be borrowed from the nature. The dolphin skin was found serving as a viscoelastic coating for delay the onset of the instability [11]. Mimicking the structure and rheology of the dolphin skin in the artificial materials gives successful coating for the drag reduction in the flows past the underwater vehicles. Several types of two-layer Kramer-like coatings have been proposed for technical applications [12] and recently the artificial dolphin skin formed by numerous papillary composed of nanotubes has been elaborated for the flow stabilization purposes [13]. The blood vessels and some other biological ducts conveying biofluids are multilayer compliant tubes composed of anisotropic viscoelastic layers. The multilayer viscoelastic wall can be used for elimination of the absolute instability of the flows in the collapsible

ducts [14,15]. The most unstable fluid based mode can be stabilized by a proper choice of the rheological parameters and thickness of separate layers [7–10]. The stabilization problem for the turbulent flow is much more difficult and in some cases may also be solved through the use of a special anisotropic viscoelasic coating [16]. Turbulent flow regime is also of a great importance for the blood flow in arteries and is responsible for the flow instability of ejection murmur, which is a negative factor affecting blood and vessel wall [17].

In the present paper ability of the isotropic and anisotropic viscoelastic multilayer composites in the steady flow stabilization through the ducts at both no stress and no displacement boundary conditions at the outer wall of the duct is studied and a series of novel results is presented.

1. Problem Formulation. The flow of incompressible Newtonian liquid in the thick-wall viscoelastic tube of circular cross-section is considered. The wall is composed of three layers with thicknesses h_1, h_2, h_3, where $h = h_1 + h_2 + h_3$ is the wall thickness. The Navier–Stokes equations for the incompressible liquid and the momentum equations for the incompressible viscoelastic layers are

$$\mathrm{div}\vec{v} = 0, \qquad \frac{\partial \vec{v}}{\partial t} + (\vec{v}\nabla)\vec{v} = -\frac{1}{\rho}\nabla p + \nu\nabla^2\vec{v} \tag{1}$$

$$\mathrm{div}\vec{u}^{\,j} = 0, \qquad \rho_w^j \frac{\partial^2 \vec{u}^{\,j}}{\partial t^2} = -\nabla p^j + \mathrm{div}\hat{\sigma}^j \tag{2}$$

where $\vec{v}, \rho, \nu$ and p are the velocity, density, kinematic viscosity and hydrostatic pressure in the fluid, $\vec{u}^{\,j}$, ρ_w^j, $\hat{\sigma}^j$ and p^j are the displacement, density, stress tensor and hydrostatic pressure for the wall layers, $j = 1,2,3$. The Kelvin–Voight model is used for the viscoelastic layers

$$\tau^j \frac{\partial}{\partial t}\sigma_i^j + \sigma_i^j = A_{ik}^j \varepsilon_k^j + \mu_w^j \frac{\partial}{\partial t}\varepsilon_i^j \tag{3}$$

where $\vec{\sigma}^{jT} = (\sigma_{rr}, \sigma_{\phi\phi}, \sigma_{zz}, \sigma_{\phi z}, \sigma_{rz}, \sigma_{r\phi})$, $\vec{\varepsilon}^{jT} = (\varepsilon_{rr}, \varepsilon_{\phi\phi}, \varepsilon_{zz}, \varepsilon_{\phi z}, \varepsilon_{rz}, \varepsilon_{r\phi})$, A_{ik}^j is the matrix of elasticity modulus, μ_w^j is solid viscosity, τ^j is the stress relaxation time, $\varepsilon_{ik}^j = (\nabla_i u_k^j + \nabla_k u_i^j)/2$. The materials of the layers are considered as orthotropic and the matrix of elasticity coefficients has the form

$$\left(A_{ik}^{(j)}\right)^{-1} = \begin{pmatrix} (E_1^{(j)})^{-1} & -\nu_{21}^{(j)}(E_2^{(j)})^{-1} & -\nu_{31}^{(j)}(E_3^{(j)})^{-1} & 0 & 0 & 0 \\ -\nu_{12}^{(j)}(E_1^{(j)})^{-1} & (E_2^{(j)})^{-1} & -\nu_{32}^{(j)}(E_3^{(j)})^{-1} & 0 & 0 & 0 \\ -\nu_{13}^{(j)}(E_1^{(j)})^{-1} & -\nu_{23}^{(j)}(E_2^{(j)})^{-1} & (E_3^{(j)})^{-1} & 0 & 0 & 0 \\ 0 & 0 & 0 & (G_1^{(j)})^{-1} & 0 & 0 \\ 0 & 0 & 0 & 0 & (G_2^{(j)})^{-1} & 0 \\ 0 & 0 & 0 & 0 & 0 & (G_3^{(j)})^{-1} \end{pmatrix}$$

where $E^{(j)}_{1,2,3}$, $\nu^{(j)}_{ik}$, $G^{(j)}_{1,2,3}$ are Young's moduli, Poisson ratios and shear moduli accordingly.

The boundary conditions include the continuity conditions for the velocities, normal and tangential components of the stress at the fluid–solid and solid–solid interfaces:

$$r = R:\ v_i = \frac{\partial u_i^1}{\partial t},\ \nu\rho V_{rz} = \sigma^1_{rz},\ \ \nu\rho V_{r\phi} = \sigma^1_{r\phi},\ -p + \nu\rho V_{rr} = \sigma^1_{rr} \tag{4}$$

$$r = R + h_1:\ u_i^1 = u_i^2,\qquad \sigma^1_{rz} = \sigma^2_{rz},\qquad \sigma^1_{r\phi} = \sigma^2_{r\phi},\qquad \sigma^1_{rr} = \sigma^2_{rr} \tag{5}$$

$$r = R + h_1 + h_2:\ u_i^2 = u_i^3,\qquad \sigma^2_{rz} = \sigma^3_{rz},\qquad \sigma^2_{r\phi} = \sigma^3_{r\phi},\qquad \sigma^2_{rr} = \sigma^3_{rr} \tag{6}$$

At the outer surface of the tube no displacement or no stress boundary conditions are considered

$$r = R + h:\ \vec{u}^3 = 0 \quad \text{or} \quad \sigma^3_{rz} = 0,\qquad \sigma^3_{r\phi} = 0,\ \ \sigma^3_{rr} = 0 \tag{7}$$

where $V_{ik} = (\nabla_i v_k + \nabla_k v_i)/2$, R and L are the inner radius and length of the tube ($R/L << 1, h/R << 1$). For the blood vessel wall the former condition corresponds to the deep intraorgan vessels attached to the surrounding tissues while the latter corresponds to the superficial vessels. In the technical units both boundary conditions can be found.

Solution of the system (1)–(7) can be sought as a superposition of the steady motion and a small axisymmetric disturbance in the form of the normal mode [6,7]:

$$\begin{aligned} \left\{\vec{v}, p\right\} &= \left\{\vec{v}^*, p^*\right\} + \left\{\vec{v}^\circ, p^\circ\right\} \cdot \exp\left(st + ikz\right) \\ \left\{\vec{u}^{(j)}, p^{(j)}\right\} &= \left\{\vec{u}^{(j)*}, p^{(j)*}\right\} + \left\{\vec{u}^{(j)\circ}, p^{(j)\circ}\right\} \cdot \exp\left(st + ikz\right) \end{aligned} \tag{8}$$

where $\vec{v}^\circ$, $\vec{u}^{(j)\circ}$, p°, $p^{(j)\circ}$ are the amplitudes of the disturbances, $k = k_r + ik_i$, $s = s_r + is_i$, s_i is the wave frequency, k_r is the wave number, s_r and k_i are spatial and temporal amplification rates. The steady part $\left\{\vec{v}^*, p^*\right\}$ of (8) is identified with Poiseuille flow.

The system (1)–(7) has been previously studied for the transversely isotropic Voight ($\tau^j = 0$) material corresponding to the blood vessel wall at the no displacement [14] and no stress [15] boundary conditions at the outer surface of the tube. The linearized ODE system for $\vec{v}^\circ, p^\circ, \vec{u}^{(j)\circ}, p^{(j)\circ}$ can be obtained from those given in [14] by substitution the matrix of elasticity modulus A^j_{ik} including $E^{(j)}_3$, $\nu^{(j)}_{23,32}$, $G^{(j)}_3$ instead of $E^{(j)}_2$, $\nu^{(j)}_{21,12}$, $G^{(j)}_2$.

2. Numerical Method. A numerical procedure to solve the fluid (1) and solid (2) equations coupled via the boundary conditions (4)–(7) has been developed. The procedure allows computations of s values for a given k number (temporal

eigenvalues) and k values for a given s number (spatial eigenvalues). The procedure consists of finding two independent solutions, to say X_1, X_2, which satisfy the boundary conditions at r=R. The components of the vectors $X_{1,2}$ are the two velocity components, the first-order derivative of the axial velocity component with respect to r and the pressure in the fluid medium. The independence of the two solutions $X_{1,2}$ is ensured by starting the computation with one of the two independent vectors formed by several values of $X_{1,2}\big|_{r=0} = X_{1,2}^0$. For instance, X_1 and X_2 can be obtained by starting the computations with the boundary conditions $X_1^\circ = (1,0,0,0)$ and $X_2^\circ = (0,0,1,0)$ accordingly. With this choice, the boundary conditions at r=0 are satisfied by both solutions X_1, X_2. It should be noted that to initiate the computation of X_1 and X_2 the chosen $X_{1,2}^0$ must form a set of free vectors, which is sufficient for the computed X_1 and X_2 to be free vectors. Then the general solution in the fluid medium is an arbitrary combination of the three free solutions, namely $X = \alpha_1 X_1 + \alpha_2 X_2$, where $\alpha_{1,2}$ are arbitrary constants.

Similarly, for the displacement field in the solid layers, we solve the linearized equations for two independent solutions, to say, $Y_1^{(k)}, Y_2^{(k)}$, k=1,2,3. The components of the vectors are the two displacement components, the first-order derivative of the axial displacement component with respect to r and the pressure in the wall layers j=1,2,3. The solution of the system (2)–(3) for the solid layers is $Y = \beta_1 Y_1 + \beta_2 Y_2$, where $\beta_{1,2}$ are arbitrary constants. The independence of the solutions $Y_1^{(k)}, Y_2^{(k)}$ is ensured by the foregoing procedure. The solutions $Y_1^{(3)}, Y_2^{(3)}$ satisfy the boundary conditions at the outer surface r=R+h. The boundary conditions at the interfaces $r = R$, $r = R + h_1$ and $r = R + h_1 + h_2$ lead to the eigenvalue problem $\hat{M}\vec{C} = 0$, where the elements of the matrix $\hat{M}$ are linear combinations of the particular solution components $X_{1,2}, Y_{1,2}^{(1)}$ and their derivatives, which involve all the rheological, geometric and hydrodynamic parameters of the system (1)–(7). The components of the vector $\vec{C}$ are the arbitrary constants $\alpha_{1,2}, \beta_{1,2}^{(k)}$. The characteristic equation is obtained by setting $\det(\hat{M}) = 0$.

The numerical procedure for solving the ODE equations based on a fourth-order Runge–Kutta method is developed. An iterative technique using the steepest decent method is developed to find the double roots of the dispersion equation $\det(\hat{M}) = 0$. The problems have a large number of material parameters and we concentrated on the effect of the viscosity, elastic moduli and thicknesses of the wall layers on the system stability for axisymmetric disturbances (n=0).

3. Results and discussions.

3.1. Temporal and Spatial Eigenvalues. In order to show the existence of absolute instability and to explain the technique devoted to its suppression, we need to determine the temporal and spatial eigenvalues of the system under consideration. Thus, we need to find k for all given s, and vise versa. As an example of the numerical computations the temporal eigenvalues in the complex s–plane for a tube composed of layers of different shear moduli are presented in Fig.1. In Fig.1a the three layers have the same rheological parameters $(G^1_{1-3}, G^2_{1-3}, G^3_{1-3}) = (1,1,1)$ corresponding to isotropic wall, while in Fig.1b–d the dimensionless shear moduli are $(G^1_{1-3}, G^2_{1-3}, G^3_{1-3}) = (5,1,1)$, $(G^1_{1-3}, G^2_{1-3}, G^3_{1-3}) = (1,5,1)$ and $(G^1_{1-3}, G^2_{1-3}, G^3_{1-3}) = (1,1,5)$ accordingly. Therefore the tube in these cases is anisotropic in the radial direction. The analysis done in [11] shows that the eigenvalues near the real s–plane axis correspond to solid-based modes, while those near the imaginary axis are the fluid-based modes. In Fig.1 one can see two groups of modes located near the real axis in the s–plane and the modes located near the imaginary axis. The density of the solid-based and fluid-based modes in the s–plane depends on the Reynolds number and the dimensionless parameter $\Gamma = \max\{v_r^*\}\sqrt{\rho / G_{ref}}$, where G_{ref} is the reference shear modulus. Note that there is only one unstable mode for the considered material parameters, while for the turbulent flows more than one unstable mode has been revealed for the same material parameters[16].

The modes playing an important role in the fluid–structure interaction are those located near the origin of the (s_r, s_i) –plane since their frequencies could match each other and their damping rates are relatively low. One of the eigenvalues has a positive real part $s_r > 0$. This is an unstable mode which we shall focus on later. A significant modification of the location of the eigenvalues in the (s_r, s_i) –plane is observed in Fig.1a–d, indicating noticeable changes in the temporal amplification rates and frequencies of the modes, notwithstanding the imposed small modification of the shear modulus of each layer. The results highlight the significant influence of the rheological parameter of each layer on stability and dynamical behavior of the system.

The spatial eigenvalues for isotropic and anisotropic tubes conveying fluid are shown in Fig.2a–d. Fig.2a shows the spatial eigenvalues for the tube composed from isotropic layers. The modes located in the upper half of the (k_r, k_i) –plane are evanescent modes that describe the response of the system in the region located after the source, i.e. if the source is located at $z = z_0$ those modes describe the behavior of the system for $z > z_0$. The evanescent modes located in the lower half of the (k_r, k_i) –plane describe the response in the

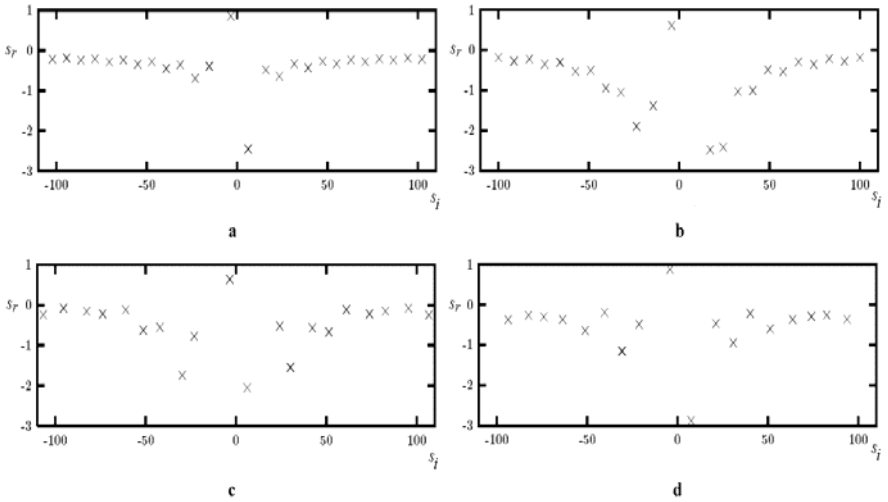

Fig. 1. Temporal eigenvalues in the complex frequency (s_r, s_i) –plane; real wave number k=2.5, Re=10, $\Gamma = 10$, non-dimensional elastic moduli $E^j_{1,2} = 3G^j$, $\rho^j_w / \rho = 1$, $h / R = 1.4$, $h_1 / R = 0.08$, $h_2 / R = 0.14$, $h3 / R = 0.08$, $\nu^j_{ik} = 0.4$, $\mu^j_w / \rho^j_w = 0$. (a): $(G_1, G_2, G_3) = (1,1,1)$ (isotropic wall); (b): $(G_1, G_2, G_3) = (5,1,1)$; (c): $(G_1, G_2, G_3) = (1,5,1)$; (d): $(G_1, G_2, G_3) = (1,1,5)$.

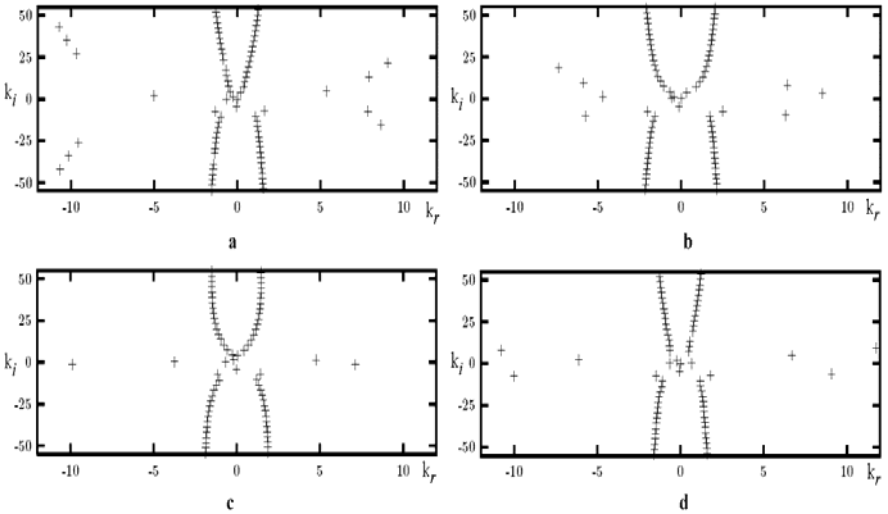

Fig2. Spatial eigenvalues in the complex wave number (k_r, k_i) –plane for the temporal amplification rate s=2i. Other parameters are the same as in Fig.1.

region located upstream of the source, i.e. in the region $z < z_0$. The sign of the imaginary part of the complex wave number k is not relevant to whether the system is stable or unstable unless it changes sign during the process of lowering the Laplace contour. In this case, the sign variation represents the system instability [7–10]. Fig.2b–d show the modification of the location of the spatial eigenvalues in the (k_r, k_i)–plane when a small change of the shear modulus of each layer is imposed. Careful examination of Fig.2a–d taking into account the scale of the figure leads to the conclusion that a small modification of the shear modulus induces a significant displacement of the eigenvalues in the (k_r, k_i)–plane, and consequently significant variations of the damping rates and frequencies of the eigenmodes.

3.2. Effect of wall viscosity on the system stability. It is found that a small increase in the viscosity of all the layers stabilizes the system, while for relatively large viscosities the system becomes unstable and the nature of the instability is again absolute. The amplification rate of the most unstable mode versus the viscosity of each layer is plotted in Fig. 3a. The group velocity of the most unstable mode versus the viscosity of the layers is presented in Fig. 3b. Note that when $\mu_r^{(2)} = 0$, the group velocity is negative. An increase in the viscosity of the first layer, which is in contact with the fluid, leads to an increase in the group velocity. In that way, the faster modes correspond to bigger viscosities. Variation of the viscosity of the third layer leads to a relatively insignificant alteration in the speed of propagation of the unstable mode. Surprisingly, any change in the viscosity of the middle layer leads to an inversion of the direction of the propagation of the unstable mode, where the group velocity becomes positive. For certain value of $\mu_r^{(2)}$, the group velocity is zero, which suggests the existence of absolute instability in the anisotropic three-layered tube.

3.3. Effect of wall rigidity on the system stability. As it was shown by the detailed numerical computations a modification of the shear modulus of the third layer does not significantly change the amplification rate and the group velocity of the unstable mode. Increasing the shear modulus of the second layer has two opposite effects in comparison to the isotropic case. The amplification rate decreases at small wave numbers (long waves); while it increases at high wave numbers (short waves), see [7, 8]. Furthermore, the wave range of unstable modes is expanded. The group velocity twice changes its sign suggesting that there are two monochromatic waves possessing zero group velocity and consequently suggesting the existence of two absolutely unstable modes of different wavelengths. Increasing the shear modulus of the first layer yields two opposite effects as well: long waves are stabilized and short ones are destabilized. In the case, the group velocity also changes sign twice, again suggesting the existence of absolute instability.

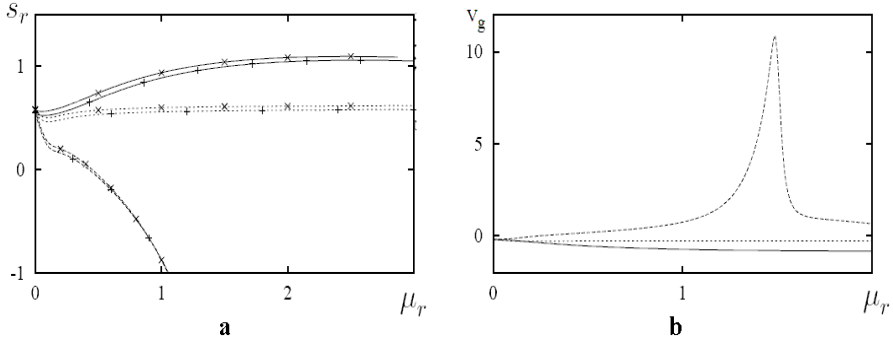

Fig. 3. (a) Temporal amplification rate of the most-unstable mode versus the viscosity of the layers for $\nu_{ik}^{(j)} = 0.1$ and $\mu_r^{(2)} = \mu_r^{(3)} = 0$ (solid line); $\mu_r^{(1)} = \mu_r^{(3)} = 0$ (dashed line); $\mu_r^{(1)} = \mu_r^{(2)} = 0$ (dotted line). The symbol + corresponds to $E_1^{(j)} = 20G^{(j)}$, $E_2^{(j)} = 2G^{(j)}$, symbol × to $E_1^{(j)} = 2G^{(j)}$, $E_2^{(j)} = 20G^{(j)}$. (b) Group velocity of the most-unstable mode versus the viscosity of the three anisotropic layers. $\nu_{ik}^{(j)} = 0.1$, $E_1^{(j)} = 20G^{(j)}$, $E_2^{(j)} = 2G^{(j)}$. Solid line corresponds to $\mu_r^{(2)} = \mu_r^{(3)} = 0$, dashed line to $\mu_r^{(1)} = \mu_r^{(3)} = 0$, and dotted line to $\mu_r^{(1)} = \mu_r^{(2)} = 0$.

Increasing the shear modulus of each of the layers corresponds to a transition from an elastic to a more rigid tube and thus stabilizes the system at relatively low values G_{1-3}^{j}. The system can also be stabilized by significant increase in the shear modulus of the outer layer. Increasing the shear modulus of the inner layer, which is in contact with fluid, reduces the amplification rate of the unstable mode. The system becomes more unstable when the shear modulus of the second layer increases. The influence of the rigidity of separate layers on the system stability has no simple explanation. The system exhibits very complex behavior and a large number of different modes, which can be realized for given geometry of the system and its rheological parameters. Certain combinations of relative thickness and rigidity of the layers can produce stabilizing or destabilizing effects on the system.

As it is shown in Fig.4–5 the system can be stabilized by a proper choice of the layered viscoelastic coating. For the no-displacement conditions the system is stabilized by rigid wall, but the effect can be reached easier by rigid outer layer (curve 4 in Fig.4a and curves 3,4 in Fig.4b) depending on the system geometry. Boundary conditions at the outer surface of the tube influence the flow stability significantly. For the no stress conditions the flow can not be stabilized by the wall rigidity (curve 1 in Fig.5 a,b). Increase in the rigidity of the outer and middle layers in combination produce the desirable effect. The system stability strongly depends on the wall rheology, geometry and flow regimes. It is

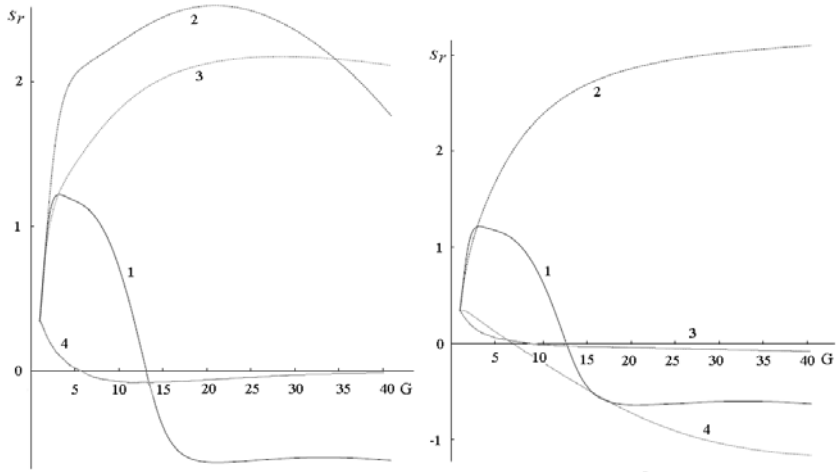

Fig.4. Temporal amplification rate of the most-unstable mode versus the shear moduli G at $k_r = 1$, Re=100, $\Gamma = 1.6$, $h = 0.6$, $h_1 = h_2 = h_3 = 0.2$, $E_{1,2}^{(k)} = E_{1,1}^{(k)} = 3G$ and no displacement boundary conditions for different sets of material parameters : $G_{1-3} = G$ (curve 1); $G_{1,2} = G, G_3 = \text{const}$ (curve 2); $G_{1,3} = G, G_2 = \text{const}$ (curve 3); $G_{2,3} = G, G_1 = \text{const}$ (curve 4) (a); $G_{1-3} = G$ (curve 1); $G_{2,3} = \text{const}, G_1 = G$ (curve 2); $G_{1,3} = \text{const}, G_2 = G$ (curve 3); $G_{1,2} = \text{const}, G_3 = G$ (curve 4) (b).

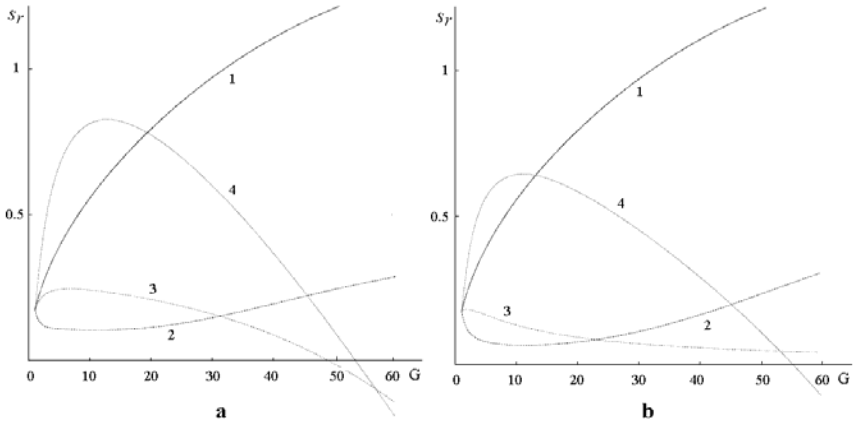

Fig.5. Temporal amplification rate of the most-unstable mode versus G for the no stress boundary conditions (collapsed tube). The sets of material parameters are the same as in Fig.4.

important that the material parameters of the successful multilayered coating for flow stabilization can be computed for different flow conditions giving a possibility for elimination the absolute instability and suppression the self-excited wall oscillations.

4. Summary. The obtained results confirm that multi-layered composites significantly influence flow stability in the compliant tubes at both no stress and no displacement boundary conditions at the outer surface of the tube. Variations of the elastic and viscous parameters of one of the layer or two layers simultaneously exert a great influence on the stable and unstable modes. In that way possible stabilizing/destabilizing effect of adaptive variations of the parameters of different layers can be analyzed. The presented results shed new light on the mechanics of the compliant wall and its role in stability/instability of the fluid flows at different boundary conditions. The set of the material parameters which provides flow stabilization can be used in biomedical and technical applications.

The work is partially supported by PICS–NASU research grant № M12–2009.

REFERENCES

1. Shapiro A.H. Steady flow in collapsible tubes // J. Biomech. Eng. – 1977. – v.99. – p.126–147.
2. Kumaran V. Stability of wall modes in a flexible tube. // J. Fluid Mech. – 1998. – v.362. – p.1–15.
3. Shankar V., Kumaran V. Asymptotic analysis of wall modes in a flexible tube revisited. // Europ. Phys. J. Ser.B. – 2001. – v.19. – p.607–622.
4. Hamadiche M., Gad-el-Hak M. Temporal Stability of flow through viscoelastic tubes. // J. Fluids Struct. – 2002. – v.16. – p.331–359.
5. Hamadiche M., Gad-el-Hak M. Spatiotemporal stability of flow through collapsible, viscoelastic tubes. // AIAA Journal. – 2002. – v.42. – p.772–786.
6. Huang L. A theoretical study of duct noise control by flexible panel. // JASA. – 1999. – v.106. – p.1801–1809.
7. Hamadiche M., Kizilova N., Gad-el-Hak M. Suppression of Absolute Instabilities in the Flow inside a Compliant Tube. // Communic. Numer. Meth. in Engin. – 2009. – v.25. – p.505–531.
8. Kizilova N., Hamadiche M., Gad-el-Hak M. Flow in Compliant Tubes: Control and Stabilization by Multilayered Coatings. // Intern. J. Flow Control. – 2009. – v.1. – p.199–211.

9. Kizilova N., Hamadiche M., Gad-el-Hak M. Flow stabilization in compliant ducts: from nature-made to human-made. // Intern. J. Numer. Meth. Applic. – 2011. – vol.6, N1. – P.1–86.
10. Kizilova N., Hamadiche M., Gad-el-Hak M. Mathematical models of biofluid flows in compliant ducts: a review. // Arch.Mech. – 2012. – v.64, N1. – P.1–30.
11. Kramer M.O. Boundary-layer stabilization by distributed damping. // J. Aeronaut. Sci. – 1957. – v. 24. – p.459–460.
12. Gad-el-Hak M. Boundary Layer Interactions with Compliant Coatings: An Overview // Appl. Mech. Rev. – 1986. – v.39. – p.511–524.
13. http://www.unr.edu/nevadanews/templates/details.aspx?articleid=4774&zoneid=40
14. Hamadiche M., Kizilova N. Temporal and spatial instabilities of the flow in the blood vessels as multi-layered compliant tubes // Intern. J. Dyn. Fluids. – 2005. – v.1. – p.1–23.
15. Hamadiche M., Kizilova N. Flow interaction with composite wall // Proc. ASME Conf. "Pressure Vessels and Piping". Vancouver, Canada. – 2006. – PVP2006-ICPVT11-93880.
16. Kizilova N., M. Hamadiche M. Stabilization of the turbulent flows in anisotropic viscoelastic tubes. // Advances in Turbulence XII. Series: Springer Proceedings in Physics, Vol. 132. Eckhardt, Bruno (Ed.), 2010. – p.899–925.
17. Sabbah H.N., Stein P.D. Turbulent blood flow in humans: its primary role in the production of ejection murmurs. // Circulat. Res. – 1976. – v.38. – p.513–525.